Journal of Applied Physics

Investigation of ultrafast excited-state dynamics at the nanoscale with terahertz field-induced electron tunneling and photon emission

Cite as: J. Appl. Phys. **133**, 110903 (2023); https://doi.org/10.1063/5.0144218
Submitted: 13 November 2022 • Accepted: 27 February 2023 • Published Online: 17 March 2023

Ikufumi Katayama, Kensuke Kimura, Hiroshi Imada, et al.

AIP Publishing

Journal of Applied Physics PERSPECTIVE scitation.org/journal/jap

Investigation of ultrafast excited-state dynamics at the nanoscale with terahertz field-induced electron tunneling and photon emission

Cite as: J. Appl. Phys. **133**, 110903 (2023); doi: 10.1063/5.0144218
Submitted: 13 November 2022 · Accepted: 27 February 2023 ·
Published Online: 17 March 2023

Ikufumi Katayama,[1,a)] Kensuke Kimura,[2] Hiroshi Imada,[2] Yousoo Kim,[2] and Jun Takeda[1,2,a)]

AFFILIATIONS

[1]Graduate School of Engineering Science, Yokohama National University, 79-5 Tokiwadai, Hodogaya, Yokohama 240-8501, Japan
[2]Surface and Interface Science Laboratory, RIKEN, 2-1 Hirosawa, Wako 351-0198, Japan

[a)]**Authors to whom correspondence should be addressed:** katayama-ikufumi-bm@ynu.ac.jp and jun@ynu.ac.jp

ABSTRACT

The combination of terahertz (THz) pulses with scanning tunneling microscopy (STM) enables us to investigate ultrafast dynamics at material surfaces with high spatial (nanoscale) and temporal (femtosecond) resolution. In this Perspective, we review the basic principles of THz-STM, outline the related literature, and discuss its future outlook capable of advancing nanoscience, especially by introducing further combination of THz-STM with scanning tunneling luminescence spectroscopy, which can extract more fruitful information about nanoscale materials via obtaining luminescence spectra compared to just observing the net tunneling current induced by THz pulses in THz-STM. By shining THz pulses onto an STM tip, we can observe plasmon luminescence locally confined between the tip and the surface, whose spectrum changes with tip conditions. The combined approach is a stepping stone toward investigating the ultrafast excited-state dynamics of nanoscale materials with high spatiotemporal resolution.

INTRODUCTION

Visualizing and manipulating the electronic properties of nanoscale materials such as atoms and molecules have been one of the fundamental goals of nanoscience for decades[1–3] as they provide a basic understanding of the structural and physical properties of materials,[4] mechanisms of chemical reactions,[5] and working principles of nanoelectronic devices.[6] Scanning probe microscopy (SPM) is a powerful experimental technique to investigate nanoscale physics and chemistry, revealing not only topographic surface structures down to the atomic resolution but also the electronic states of molecules and surface states, as well as thermal, electronic, magnetic, and mechanical properties with suitable selections of probing schemes, as shown in Fig. 1(a).[2,7–27] These capabilities of SPM have flourished surface sciences by means of many beautiful visualizations and manipulations of nanoscale materials and applications to the investigation of material properties.[4,15,17]

Among the various experimental techniques of SPM, scanning tunneling microscopy (STM) is particularly advantageous[7] in that a sharp metal tip with a curvature at the nanoscale is used to induce a tunneling current between the sample and the tip. Because the tunneling probability of electrons transmitting through the nanoscale gap between the sample and the tip is extremely nonlinear, subtle changes in the tip–sample distance drastically affect the magnitude of the tunneling current flowing between them.[28] For example, only a 10% change in the tip–sample distance (0.1 nm) approximately leads to an order of magnitude change in the tunneling current. This extreme enhancement of the signal enables us to precisely map and control the height of the tip and obtain surface images with atomic resolution.[15] The tunneling current also strongly reflects the surface density of states (DOS), revealing the images of energy-resolved wave functions at the surface.[29] Thus, the SPM techniques that make use of the strong nonlinearity of the tunneling current can realize a high spatial resolution.

In contrast to the high spatial resolution of STM, the temporal resolution is limited by the bandwidth of the electronic circuit, such as a current amplifier, or the scanning speed. The bandwidth of the electronics used in STM is typically in the kHz range,

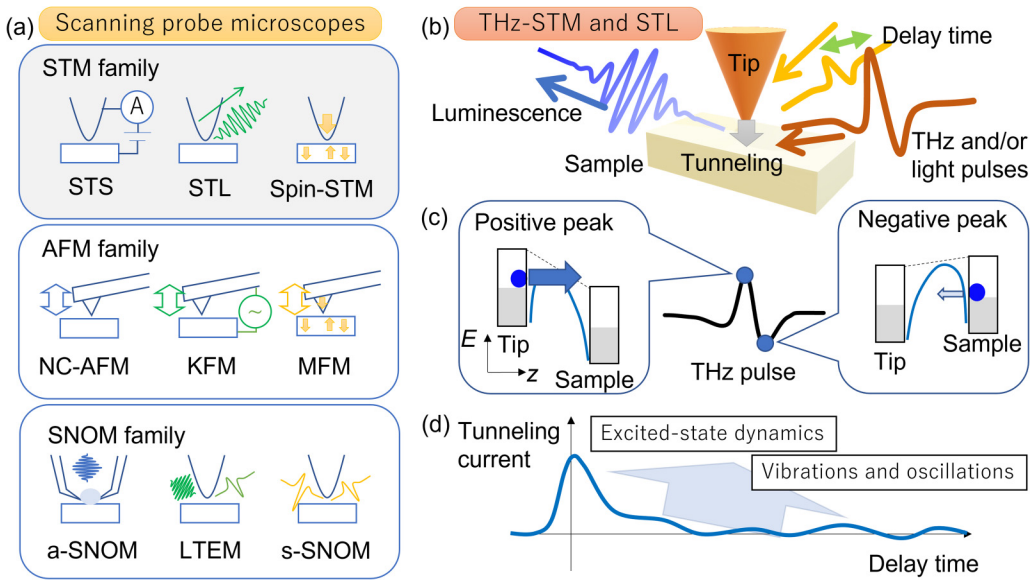

FIG. 1. Various types of scanning probe microscopes (SPMs) and the overview of THz-STM and STL spectroscopy. (a) Types of scanning probe microscopes (SPMs). There are three families of the SPM, scanning tunneling microscopy (STM),[7] atomic force microscopy (AFM), and scanning near-field microscopy (SNOM), some of which are already combined with terahertz technology to reveal nanoscale ultrafast dynamics. For the STM family, there exists scanning tunneling spectroscopy (STS)[13,15] to reveal electronic states, scanning tunneling luminescence (STL) spectroscopy[7,25,58] to investigate excited states, and spin-polarized STM (Spin-STM)[4,5,10,23] to visualize the magnetic texture at the nanoscale. For the AFM family,[2,15,16,18,20] there are noncontact (NC) AFM[22] to visualize surface morphology, Kelvin force microscopy (KFM)[11,14,19] to investigate electronic properties, and magnetic force microscopy (MFM)[8,10,26] to investigate magnetic properties. For the SNOM family, there are aperture-type SNOM[12,23] to resolve optical properties, laser-induced terahertz emission microscopy (LTEM)[11,14,19,26] to investigate terahertz generation, and scattering-type SNOM[6,8,16,18,22,21] to visualize nano-optical responses. (b) Schematic of THz-STM and STL. (c) Electron tunneling induced by the terahertz electric field. The higher field strength (positive peak in this case) induces much more tunneling electrons to be observed by the current measurement. (d) Schematic of a typical waveform obtained by the optical pump and the THz-STM probe experiment.

corresponding to a time resolution of milliseconds.[30,31] However, this limitation can be overcome with the use of ultrashort pulsed lasers.[32] Instead of measuring the time evolution of the tunneling current directly, researchers shined ultrashort optical double pulses onto an STM tip and observed tunneling current variations as a function of the time interval between the pulses.[32,33] The ultrafast dynamics of photoexcited carriers were investigated using this technique. However, the interpretation of the observed signal is difficult since the optical excitation indirectly contributes to the change in the tunneling current, and many complex processes (e.g., electronic and thermal excitations) are involved in the results.[34]

In terahertz (THz) time-domain spectroscopy, THz pulses are generated by the optical rectification of ultrashort laser pulses in electro-optic crystals, photoconducting antennae, and other devices for THz generation; thus, the electric field waveform is phase-locked and invariant for each pulse.[35–37] THz pulses shined onto the STM tip can induce bias modulation owing to the strong field enhancement at the gap between the sample and the tip,[38,39] generating an observable tunneling current if the I–V curve possesses high nonlinearity and the modulation is sufficiently strong [Figs. 1(b) and 1(c)]. The induced tunneling current is normally measured in THz-STM experiments.

Because the tunneling current in THz-STM only flows when the THz pulse is applied, the current can be temporarily localized, offering us an extremely high time resolution.[38,40] Furthermore, because of the broad bandwidth of THz pulses, the waveform can form a monocycle, which is useful for increasing the temporal resolution. The method can realize the observation and manipulation of the ultrafast dynamics of electrons at the nanoscale and can be applied to develop electronic nanodevices. Notably, the energy of THz pulses (~4.2 meV and ~48 K) is small compared to the infrared or visible light (~1 eV and ~10^4 K), enough to reduce the thermal effects on tip–sample interactions. The related Keldysh parameter, which characterizes light–matter interactions, becomes smaller than 1 because of the small carrier frequency of THz pulses, meaning that the induced current is due to the tunneling process rather than multiphoton excitations. Therefore, the process involved in the generation of the tunneling current is only the ultrafast modulation of the bias voltage between the tip and the sample, which is rather simple and can easily be interpreted in comparison with STM combined with ultrashort pulsed lasers.

Here, we briefly review the history of THz-STM. A more detailed review of THz-STM can be found elsewhere.[41,42] A seminal demonstration of the combination of THz pulses with STM was reported in 2013 by Cocker *et al.*, and the ultrafast dynamics of excited electrons in semiconductor nanoparticles were demonstrated.[38] A few years later, observations of molecules and semiconductor surfaces using THz-STM followed, demonstrating

the possibility of inducing coherent molecular motion and manipulating electron tunneling.[39,40,43] In addition, the dynamics of vibrational, electronic, and photoexcited states of materials at the nanoscale are investigated by several groups using THz double pulses[40,44,45] or optical pump and THz-STM probe spectroscopy[46,47] [Fig. 1(d)]. The switching action of a single molecule and the atomic-scale THz waveform sampling were also reported.[48–50] Recently, the time resolution of THz-STM (or lightwave-driven STM) was improved by replacing THz pulses with either near-infrared (NIR) or mid-infrared (MIR) phase-locked light pulses.[51–56]

In this Perspective, we review the basic principles of THz-STM and outline the related literature. Then, we focus on THz scanning tunneling luminescence (STL) spectroscopy as a promising method to visualize the ultrafast excited-state and charged-state dynamics of the localized states, such as defects, impurities, molecules, and nanomaterials.[57] In contrast to THz-STM and THz-STS where tunneling spectroscopy relies on changes in the bias voltage applied to the sample, STL spectroscopy can provide more fertile information about the excited states by adding another axis of information via the measurement of intensity, energy spectrum, and polarization of luminescence induced by electron tunneling.[27,58,59] Thus, the combination of THz-STM and STL spectroscopy is envisioned to advance the experimental investigation of the excited-state dynamics at the nanoscale in the future.

FUNDAMENTALS OF THz-STM

In conventional STM, the tip–sample voltage is applied to induce the tunneling current, which is then measured with a current amplifier. The current is stabilized by changing the tip–sample distance using a feedback loop. While scanning the xy position of the tip on the surface, the z-position of the tip or the sample is recorded and plotted to show the nanoscale surface image (this is so-called the constant current mode). The working principle of THz-STM is very similar, except that the bias voltage is modulated by THz pulses. The voltage between the tip and the sample varies on an ultrafast timescale; thus, the full temporal waveform of the applied THz pulses must be considered to estimate the total tunneling current.[60] Because the tunneling time is known to be extremely fast, much less than a femtosecond,[61] electron tunneling can be regarded as instantaneous in the THz frequency region. However, the micrometer-scale tip–sample configuration significantly modifies the local THz waveform confined to the gap.[62] Some methods have been proposed to estimate the local electric field, which indicates the importance of retrieving an inherent THz waveform at the gap over the distortion or the phase shift of the THz waveform coming from the microscopic tip–sample configuration.[46,49]

Once a local electric field waveform is obtained, the total current induced by the THz electric field can be calculated as follows: First, the tunneling probability $T(E,\ s)$ between the tip and the sample can be derived under the Wentzel–Kramers–Brillouin (WKB) approximation[60]

$$T(E,\ s) = \exp\left(-\frac{2}{\hbar}\int_{z_1}^{z_2} dz\sqrt{2m(V(z,\ s) - E)}\right). \quad (1)$$

Here, E is the energy of electrons, s is the gap distance, m is the mass of an electron, and $V(z,\ s)$ is the shape of the potential barrier between the tip and the sample. The integral runs between z_1 and z_2, which is the boundary of the region that satisfies $V(z,\ s) > E$. When we apply the bias voltage V_{bias} between the tip and the sample, the tunneling current $J(V_{\text{bias}},\ s)$ can be written as

$$J(V_{\text{bias}},\ s) = \frac{4\pi e}{\hbar}\int_0^{eV_{\text{bias}}} dE\rho_{\text{tip}}(E - eV_{\text{bias}})\rho_{\text{sample}}(E)T(E,\ s). \quad (2)$$

The parameters $\rho_{\text{tip}}(E)$ and $\rho_{\text{sample}}(E)$ correspond to the DOS of the tip and the sample at a given energy E, respectively. Because s and V_{bias} are in the exponent of Eq. (1), the tunneling current is extremely sensitive to variations in these parameters, enabling us to map the material surface with atomic resolution.

In THz-STM, THz pulses modulate the voltage between the tip and the sample. Thus, the total bias voltage can be written as the summation of the direct current (DC) bias voltage and the THz field, $V_{\text{bias}}(t) = V_{\text{DC}} + V_{\text{THz}}(t)$, which changes on ultrafast timescales. The magnitude of the net tunneling current induced between the tip and the sample is

$$J_{\text{total}}(s) = f_{\text{rep}}\int_0^T dt\ J(V_{\text{bias}}(t),\ s), \quad (3)$$

where f_{rep} denotes the repetition rate of THz pulses. Because the induced current reflects electrons that tunnel through the gap, it depends not only on the peak electric field strength of THz pulses but also on the current–voltage (I–V) characteristics of the sample, as shown in Fig. 2, where the applied THz electric field waveform (a) and the I–V curve (b) are plotted.

The tunneling current can be calculated using the I–V curve and Eq. (3) as plotted in Fig. 2(e). To estimate the energy distribution of THz-induced tunneling electrons (or the energy resolution), we can introduce the total time interval instead when a certain bias voltage is applied. This can be calculated as

$$D(V) = \int_0^T dt\ \delta(V - V_{\text{bias}}(t)). \quad (4)$$

The result is shown in Fig. 2(c), obtained by summing the inverse of the time derivative of the THz waveform. We call $D(V)$ the density of time (DOT) from the analogy of DOS in condensed matter physics. The current can be calculated by multiplying DOT with the I–V curve, as shown in Fig. 2(d). Then, we can obtain the energy spectrum of tunneling electrons that determines the energy resolution of the THz-STM system. The integration of the current through the voltage [vertical axis of Fig. 2(d)] directly corresponds to the observed total tunneling current, which is the observable parameter in the THz-STM experiment.

In addition to the energy resolution, the time resolution of THz-STM is of crucial importance. The resolution estimation can be easily performed by calculating the time dependence of the tunneling current using the I–V curve shown in Fig. 2(e). Owing to the high nonlinearity of the I–V curve, the pulse width of the THz-induced current becomes shorter than the applied THz

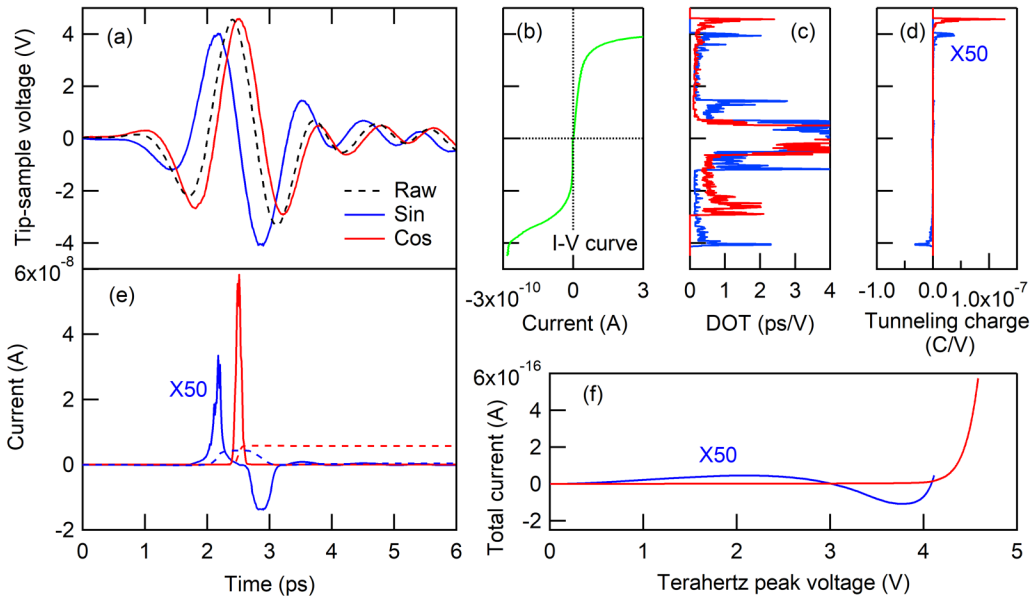

FIG. 2. Typical terahertz waveforms and the estimation of terahertz-induced current. (a) Terahertz waveforms with different phase offsets. The dashed line is the raw terahertz waveform observed at the far field, and the waveforms with the same spectrum but with purely cosinusoidal and sinusoidal phases are also plotted. The vertical axis is converted to the tip–sample voltage by assuming the field enhancement factor of 10^5 between far and near fields. (b) Current–voltage (I–V) characteristic obtained for the Au tip and Ag (111) surface configuration. (c) Density of time (DOT) of the terahertz waveforms plotted in (a). (d) Energy distribution of the tunneling current obtained by multiplying (b) and (c). The tunneling current mostly flows at the timing of the highest tip–sample voltage. (e) Estimated time dependence of the tunneling current. The dashed lines show the net current induced by the terahertz pulses obtained by integrating the solid lines. (f) Dependence of the tunneling current as a function of terahertz peak electric field strength. Both the magnitude and dependence of the tunneling current on the peak field drastically change depending on the phase of the terahertz waveforms. The repetition rate of the laser was assumed to be 100 kHz.

waveforms. As shown in Fig. 2(e), the calculated pulse duration of the tunneling current is much shorter than the period of THz oscillation, reaching 200 fs in this case. As mentioned above, the time and energy resolutions depend on both the degree of nonlinearity of the I–V curve and the amplitude of the applied THz electric field.

In the case of a strong nonlinear I–V curve, as shown in the high-voltage region of Fig. 2(b), the THz-induced tunneling current strongly depends on the phase of THz pulses. The THz pulse with the co-sinusoidal waveform plotted as the red line in Fig. 2(a) can induce a much more observable net direct current between the tip and the sample than that with the sinusoidal (the blue line), as shown in Figs. 2(f) and 2(e).[39,62] Therefore, to understand the characteristic of the sample, we need to carefully evaluate the I–V curve, the local electric field waveform, and the field strength.[60,63] A tip–sample voltage of 4 V yielded small tunneling currents, as shown in Fig. 2(f), using laser sources at a 100 kHz repetition rate.

The total current described by Eq. (3) includes the factor of the repetition rate of THz pulses. Therefore, if the current-induced phenomenon is repeatable, it would be better to utilize THz pulses generated by a laser source with a high repetition rate, which yields more current. Furthermore, it is required to modulate the tip–sample voltage at which the I–V curves exhibit strong nonlinearity. Thus, a powerful laser and an efficient THz generation method are required to generate strong THz pulses with a high repetition rate.[44,64–66] Recent developments in laser technology, such as Yb fiber lasers,[67,68] enable us to integrate new approaches in the THz-STM field owing to the simultaneous realization of high pulse energy and high repetition rate.[69]

One important difference between THz-STM and the conventional STM with a DC bias (DC-STM) is the dependence of current on the applied voltage. In DC-STM, a linear response of electron tunneling can be observed, such as the contact resistance. On the contrary, a linear response of the tunneling current is difficult to be observed in THz-STM, as shown in the low bias region of Fig. 2(f). This is because THz pulses that travel through free space do not carry the DC component, and the linear I–V curve near the zero bias totally cancels out contributions from the positive and negative electric fields, generating no net current between the tip and the sample (a similar cancellation effect is also observed in sinusoidal waveforms, as shown in Fig. 2, which have the same peak electric field strengths for positive and negative polarities). Therefore, THz-STM is unsuitable for measuring the linear response but is very sensitive to the nonlinearity area of the I–V curve. This characteristic can be useful for observing the nanoscale dynamics of the electronic states. Because the applied THz waves are pulsed and the tunneling current is temporally localized, as shown in Fig. 2(e), we can observe the ultrafast dynamics of transient occupation and the energy shifts of the electronic states, such as band renormalizations, dynamic Stark shifts, etc. by measuring

the dependence of the THz-induced tunneling current on the delay time between the optical and THz pump pulses.

Based on these considerations, the following points must be considered to design THz-STM experiments:

1. Determination of the electric field strength required for observing the energy range of interest from the I–V curve of the target sample.
2. Estimation of the required output power and the repetition rate of the laser to simultaneously realize the required electric field strength and the observable magnitude of the current.
3. Determination and control of the THz waveform both in phase and amplitude.

Once the tunneling current is observed, it becomes possible to investigate nanoscale dynamics by changing the delay time between pulses. Notably, the tunneling current can be increased by adjusting the distance between the tip and the sample. The small magnitude of the tunneling current shown in Fig. 2(f) can be improved by reducing the tip–sample distance because both the distance and the voltage, which exist in the exponent of Eq. (1), contribute to the tunneling probability.[60,70]

PHYSICAL INFORMATION OBTAINED FROM THz-STM EXPERIMENTS

THz-STM can be used to monitor the dynamical properties of materials at the nanoscale. Since carriers can be excited with near-infrared or visible pulses, THz-STM can detect the dynamics after photoexcitation by observing changes in the THz-induced tunneling current. This approach was demonstrated in an earlier report[38] in which semiconductor nanodots were photoexcited by optical pulses at 800 nm; then, the THz-induced tunneling current was measured using the THz-STM setup shown in Fig. 3(a).

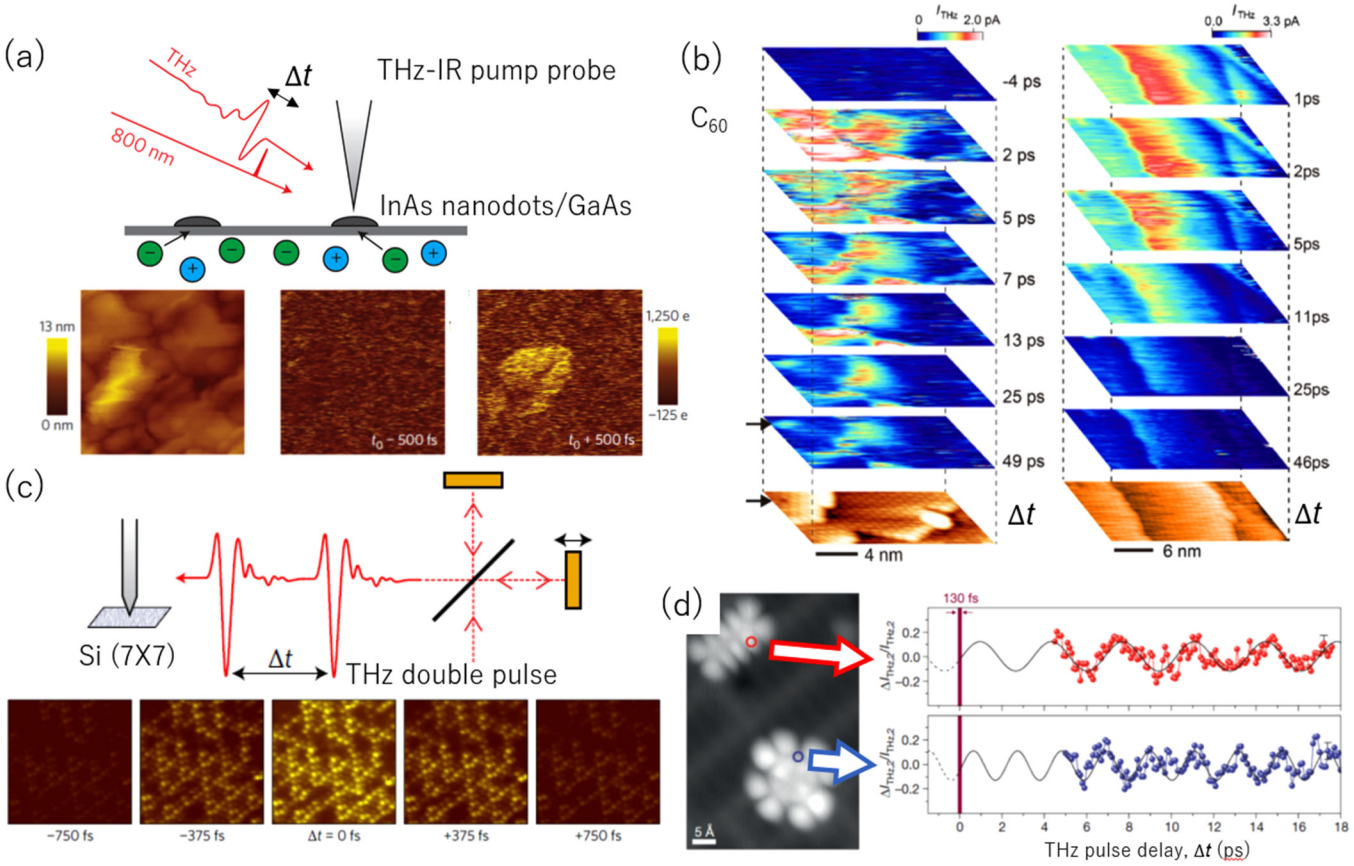

FIG. 3. Some examples of THz-STM measurements. (a) Optical pump and THz-STM probe measurements of semiconductor nanodots.[38] Reproduced with permission from Cocker *et al.*, Nat. Photonics **7**, 620 (2013). Copyright 2013 Springer Nature. (b) Two-dimensional dynamical image of the optical pump and THz-STM probe spectroscopy that measures the relaxation dynamics of the photoexcited states at the nanoscale.[47] .From Yoshida *et al.*, ACS Photonics **8**, 315 (2021). Copyright 2021 Author(s), licensed under a Creative Commons Non-Commercial No Derivative Works Attribution (CC-BY-NC-ND) license. (c) THz-STM of the silicon 7 × 7 reconstructed surface measured by the terahertz double pulses.[43] Reproduced with permission from Jelic *et al.*, Nat. Phys. **13**, 591 (2017). Copyright 2017 Springer Nature. (d) Measurement of molecular vibrations on the surface adsorption potential using terahertz double pulses.[40] Reproduced with permission from Cocker *et al.*, Nature **539**, 263 (2016). Copyright 2016 Springer Nature.

Photoexcited electrons had higher energies than valence band electrons; therefore, they were easier to tunnel out from the sample by the THz electric field. The lifetime of the excited state, spatial distribution, and the dynamics of the surface potential can be evaluated by measuring the amount of the THz-induced tunneling current as a function of delay time between the pump and probe THz pulses because the photoexcitation locally creates charge distribution (or conduction band electrons). One of the recent examples of ultrafast microscopic investigation of the surface dynamics is also shown in Fig. 3(b),[47] where the local population of photoexcited electrons in C_{60} multilayers is directly visualized. The dynamics of the population mapped with nanoscale and femtosecond resolutions demonstrated an important advantage of THz-STM.

Another interesting capability of STM is the atomic-scale resolution due to the extreme nonlinearity of the tunneling current with the tip–sample distance. If the tip used in STM is sufficiently sharp, only a couple of atoms on top of the tip contribute to electron tunneling, making STM sensitive to the roughness of the surface at the atomic scale. Whether this atomic resolution remains in THz-STM or not is another milestone, which is demonstrated using the reconstructed silicon surface shown in Fig. 3(c).[43] The spatial resolution of the microscope was comparable to or slightly better than the conventional DC-STM if the current flow was sufficiently low to keep the tunneling channel localized at the atomic scale. When THz-STM is driven by double pulses, the vibration of an adsorbed molecule at the surface could even be investigated in the time domain, as shown in Fig. 3(d).[40,70]

Furthermore, manipulating electron tunneling and controlling material properties at the nanoscale by THz pulses is another research direction. Although the control of the phases and structures of materials using THz-STM has not been demonstrated to date, the control of the THz waveform is indispensable for this purpose because the tunneling current strongly depends on not only the amplitude but also the phase of THz pulses, as shown in Fig. 2. Various experimental techniques such as the Guoy phase shift,[39] the carrier-envelope-phase (CEP) shifter,[62] and the combination of mirrors[70] were proposed to control the phase of THz waveforms. The THz-STM measurements using these phase control techniques revealed the capability of THz-STM to manipulate the direction of electron tunneling on ultrafast timescales,[39] verifying that THz-STM undertakes field-induced phenomena rather than trivial thermal effects. These approaches pave the way for controlling the physical and chemical properties of nanomaterials on ultrafast timescales by applying a high electric field on the sample and injecting or retracting many electrons to or from the sample.[43]

To improve the temporal resolution of STM, several groups utilized the NIR or MIR pulses instead of THz pulses.[51,53–56] The problem for combining NIR or MIR pulses with STM is the small enhancement factor at the gap, which originates from the shorter wavelength of the NIR or MIR pulses compared with the THz wavelength.[52] Normally, the STM tip has an apex with a size of a few hundred micrometers, and the resonance of the microstructure typically exists at the THz region. Because the enhancement factor of the electric field at the gap roughly scales with the wavelength when it is shorter than the structural resonance of the tip, the electric field strength required to induce the tunneling current becomes higher at a shorter wavelength (i.e., short pulse duration). However, electromagnetic waves with shorter wavelengths can be focused tightly and thus can overcome the reduction of the field enhancement factor. Some experimental trials of light-field-driven STM using MIR or NIR pulses[53,54] achieved a much faster time resolution of THz-STM. The shorter time resolution opens possibilities to investigate ultrafast phenomena, such as energy transfer, coherent phonon excitation, and phase transitions.[45,71,72]

The findings reviewed here mainly focus on the observation of the THz-induced current, which is the summation of all changes occurring at the tip–sample gap. The integration, however, may obscure the underlying physics of the THz-induced phenomena. The observation of physical quantities other than the tunneling current can resolve this limitation. In SPM, various experimental methods can be applied to investigate surface properties, as shown in Fig. 1, which can be useful for obtaining new dynamical information if combined with THz pulses.[73] For example, in THz scanning near-field microscopy (SNOM),[41,42] the scattering or the emission of THz waves is detected with an oscillating AFM probe, which can be used to observe the nanoscale physical and optical properties of materials.[11,12,14,19,23,26]

More importantly, the absence of the net tunneling current does not mean that THz pulses induce any effect on the sample, as reported using THz-induced force microscopy by Peller *et al.*[48] They showed that the switching of adsorbed molecular configuration is induced by THz pulses with smaller electric field strength than that for observing the THz-induced tunneling current.[48] It may be useful to combine THz-STM with other probes to observe such changes without detecting the tunneling current. Among them, we introduce THz-STL spectroscopy, which can provide a new approach to investigating the excited-state dynamics at the nanoscale.[58,59]

THz-STL SPECTROSCOPY FOR ULTRAFAST EXCITED-STATE DYNAMICS

As discussed in the previous sections, THz-STM can introduce femtosecond time resolution to STM, which offers nanoscale or even atomic-scale spatial resolution.[38–43,47] Thus, the ultrafast dynamics in various systems such as semiconductors, molecules, surface defects, impurities, and nanomaterials can be investigated using THz-STM with high spatiotemporal resolution.

However, observation of the THz-induced tunneling current is generally not sufficient for revealing the overall ultrafast dynamics occurring at a nanometer scale. The electron tunneling can trigger luminescence emitted from the excited states of the target materials, which may give useful information on dynamics, in devices such as organic light-emitting diodes and photovoltaic cells. Thus, the combination of luminescence spectroscopy with STM is of particular importance. Although sophisticated techniques such as single-photon correlation spectroscopy of DC-STL or nanosecond STL have been already installed,[74–76] time-resolved experiments with higher temporal resolution are out of reach. For this purpose, we could combine THz-STM with STL, analogous to the terahertz-induced luminescence spectroscopy reported in semiconductors and nanomaterials.[77,78]

STL spectroscopy is a powerful measurement scheme of STM in which tunneling electrons deposit energy to the sample through

charge injection or to the plasmon mode at the tip–sample interface through inelastic scattering.[59,79–81] The resultant luminescence can be observed in the far field, and its spectrum can be resolved using a conventional spectrometer, giving us fruitful information on energy dissipation/conversion of the target materials. Because the process is triggered by electron tunneling at the nanoscale gap between the tip and the sample, and by inelastic scattering through atomic-scale plasmonic picocavities,[82,83] we can achieve high spatial resolution in STL experiments and reveal the relation between luminescence and the electronic wave function of the relevant electronic states.[84] This characteristic of STL spectroscopy enables us to investigate the nanoscale energy transfer, energy dissipation, etc., which involve unique information on single molecule dynamics.[58]

An example of the DC-STL experiment is shown in Fig. 4(a), where phthalocyanine (Pc) molecules were are adsorbed on a 3-monolayer NaCl crystal deposited on a silver (111) substrate.[58] The insulating layer (NaCl) was inserted in between the molecule and the metal substrate because the molecule must be isolated from the metal to suppress the energy transfer of the excited electrons to the substrate. The spectra shown in Fig. 4(a) are obtained at the indicated tip positions on the isolated molecules and molecular dimers. The luminescence band of H_2Pc was observed at 1.81 eV, and that of MgPc was observed at 1.88 eV.

The luminescence spectrum of the dimer originated from the combination of MgPc and H_2Pc molecules, although the MgPc molecule was selected for STL excitation. Depending on the relative position of MgPc and H_2Pc molecules, the luminescence from H_2Pc was observed even after the excitation of the MgPc molecule, indicating the intermolecular energy transfer from MgPc to H_2Pc. Thus, STL spectroscopy can reveal such intermolecular energy transfer between luminescent molecules with atomic-scale spatial resolution.[27,58,85] The spatial distribution of luminescence intensity, which involves versatile information not only on the wave function of the relevant luminescence band, but also on the fine excited-state structures such as vibronic states can also be investigated.[84] Thus, visualizing nanoscale luminescence properties is being extensively

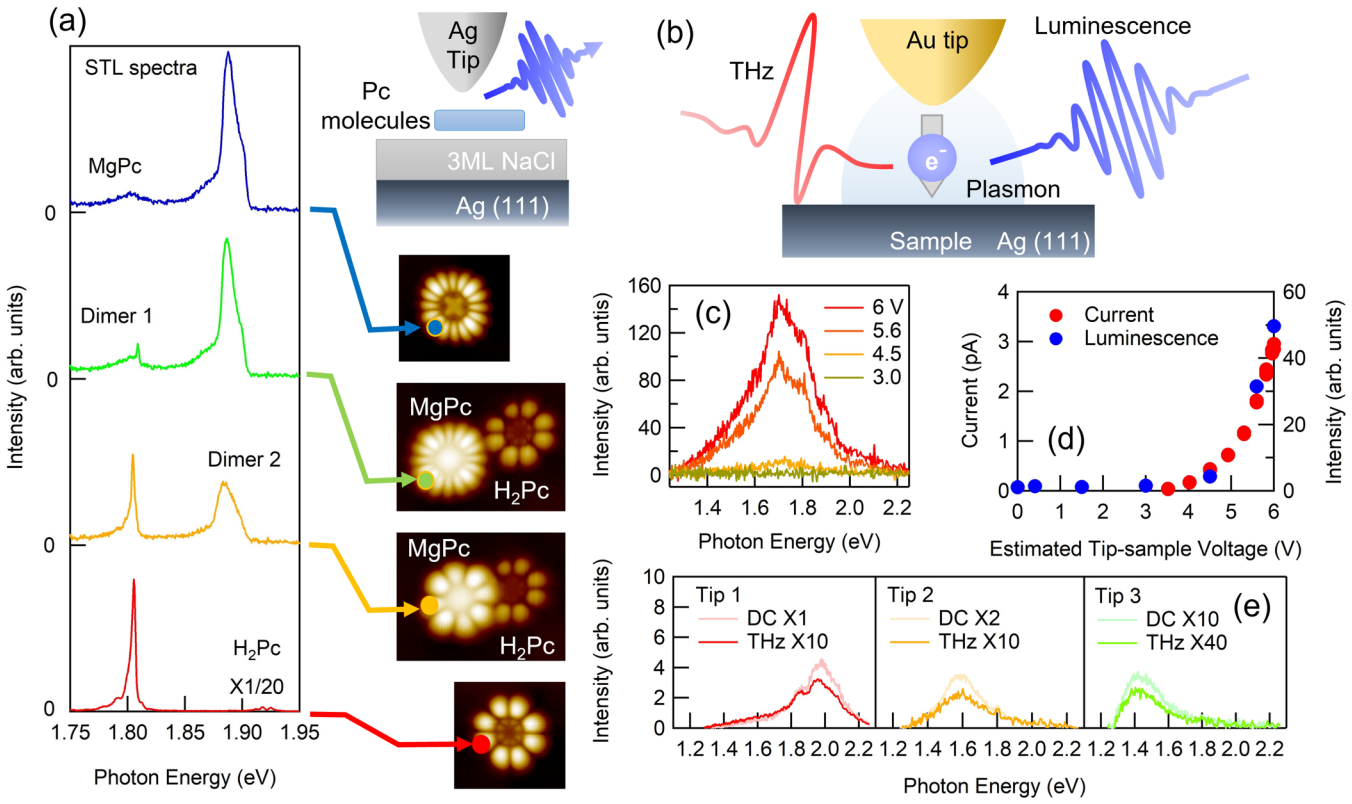

FIG. 4. STL and THz-STL results. (a) STL spectra of Mg- and H_2-phthalocyanine molecules and dimers.[58] The luminescence spectra were obtained at the indicated tip positions on the topographic STM images. An illustration of the sample configuration is also shown on top of the figure. (b) Schematic of the terahertz STL setup. The terahertz wave was applied to induce electron tunneling between the tip and the sample, and the luminescence emitted from the surface was observed. Note that the tip is placed directly on the metal substrate in (c)–(e). (c) Dependence of the spectra of terahertz-induced plasmon luminescence on estimated peak tip–sample voltages.[57] The peak electric field strength of the applied terahertz wave was approximately 200 V/cm, which corresponded to the tip–sample voltage of 6 V. The red, orange, and yellow curves correspond to the data with the three highest luminescence intensities plotted in (d). (d) Dependence of the tunneling current and luminescence intensity on the peak tip–sample voltages. (e) THz and DC tunneling luminescence of three different tip configurations, showing that THz-STL originated from plasmon luminescence.[57]

investigated, which may be useful for designing future organic semiconductor light-emitting diodes and transistors.[17,59,86]

To investigate energy transfer and dissipation processes with molecular systems in the time domain, a combination of THz-STM and STL spectroscopy can be a promising solution, as shown in Fig. 4(b). By harnessing this scheme, we first investigated the tunneling current-induced plasmon luminescence locally confined at the tip–sample position on a metal surface without any molecules.[57] The result is shown in Figs. 4(c)–4(e). When applying THz pulses with a 200 V/cm peak electric field strength and a 100 kHz repetition rate, we induced a tunneling current of 3 pA, as shown in Fig. 4(d). The tip–sample voltage induced by a THz pulse was ~6 V as a result of the electric field enhancement factor of $\sim 3 \times 10^5$, which was estimated using the model described in previous sections.[39] Note that the estimated voltage is significantly higher than that used in the conventional STL measurements shown in Fig. 4(a) because a higher voltage is required to induce a sufficient tunneling current for THz-STL observation with a 100 kHz repetition rate. Luminescence intensity as a function of the maximum tip–sample voltage induced by THz pulses shown in Figs. 4(c) and 4(d) behave in a similar manner as that of the tunneling current, indicating that luminescence originates from tunneling electrons as in the conventional STL measurements.

Figure 4(e) also shows the obtained experimental results of THz-STL measurements by changing the tip conditions using different plasmon resonances. The conditions were adjusted by applying a high pulsed voltage to the tip, and plasmon resonances change owing to the nanoscale changes of the tip apex. The obtained spectral shapes corresponded well to those observed in DC-STL measurements. The similarity of the spectra indicates that the origin of luminescence observed in THz-STL is the plasmons at the surface excited by tunneling electrons. The intensity of THz-STL is much weaker than that of DC-STL with the same tunneling current. A possible reason for the intensity difference is the reduced emission efficiency at the high bias voltage. In the THz-STM experiment, most of the tunneling electrons have high energy, as shown in Fig. 2(d), where the emission efficiency is small compared to the lower bias voltages used in the DC case. As a result, the plasmon luminescence in the THz-STL measurement becomes much weaker than that in the DC-STL measurement.

The observation of the plasmon luminescence through THz-STM indicates the possible use of future THz-STL measurements for the characterization of various materials. The luminescence, which is triggered by either electron injection or retraction, provides valuable information on the excited states, such as the intensity, energy spectrum, and polarizations of the emitted photons. By analyzing the obtained spectral information, energy dissipation of the excited states, energy transfer to neighboring sites, and the formation processes of the charged or excited states can be investigated. Possible experiments that can be performed using THz-STL are summarized in Fig. 5. The ultrafast tunneling process due to THz pulse excitation allows us to investigate the picosecond, nanosecond, and microsecond decay dynamics of the excited states using time-domain techniques, such as double-pulse excitation, the use of a time-to-amplitude converter, a streak camera, and so on.

In THz-STL, excited states can be generated either by one-step charge injection to a charged molecule [Fig. 5(a)][59] or two-step charge injection to a neutral molecule [Fig. 5(b)]. We can change the energy of the injected electrons by changing the electric field strength and carrier-envelope phase of the applied THz pulses. Then, the time-resolved experiment of luminescence can track energy dissipation dynamics after the formation of the excited states. If we change the time interval between the double pulses in the latter case [Fig. 5(b)], the formation process of the excited states may also be revealed in the femto- or pico-second timescale. The obtained information can be useful for understanding the initial charging dynamics and energy relaxation.

Another interesting possibility is the use of plasmons or magnetic tips to excite luminescence in THz-STL, as shown in Figs. 5(c) and 5(d). The plasmon excitation summarized in Fig. 4 can be used as the excitation photon of luminescence. As shown in Fig. 5(d), we can also realize spin injection to the sample using a magnetic tip (see also Fig. 1), which is promising for investigating polarization and spin dynamics via the detection of polarization-dependent luminescence.[87] Furthermore, if an optically active localized luminescent center exists, the luminescence efficiency may change when moving the tip position, providing spatiotemporal information and the diffusion of the excited states.

Despite these promising possibilities, the THz-STL spectroscopy of single molecules, surface defects, impurities, or nanomaterials has yet to be reported, possibly because of the low frequency of luminescence. To generate THz pulses with sufficient electric field strength to induce tunneling, high pulse energy of the laser for THz generation is required, limiting the repetition rate of THz pulses, and resultantly, the luminescence. Furthermore, the electric field strength must be reduced to operate THz-STL at lower bias voltages where efficient single-molecular luminescence is observed, and the molecules must be kept unchanged without any damage even when a high bias voltage is applied instantaneously by THz pulses. However, the tunneling current nonlinearly decreases with the decreased electric field strength (bias voltage); therefore, it becomes difficult to observe luminescence in such a condition. To observe luminescence at a single molecule level, we may control another degree of freedom that can enhance the tunneling current, i.e., the tip–sample distance. If the tip approaches the sample by 10% (~0.1 nm), the tunneling current increases by one order of magnitude. This can prevent the decrease in the tunneling current and may make it possible to observe luminescence even at low bias voltages with THz-STL spectroscopy.

Ammerman *et al.* utilized THz-STM with an extremely narrow tip–sample distance to observe the wave functions of graphene nanoribbons at the atomic scale.[70] They increased the total current induced by THz pulses by several orders of magnitudes. Increasing the repetition rate of THz pulses also contributed to the high sensitivity obtained in the detection of the THz-induced tunneling current because the number of pulses per unit time and the net tunneling current can be increased.[44,60] By combining these schemes, it might also be possible to induce molecular luminescence, allowing us to measure the ultrafast dynamics of the excited states in a single molecule.

Overall, precise tuning of the THz waveform and tip–sample conditions will enable us to control electrons to be either injected

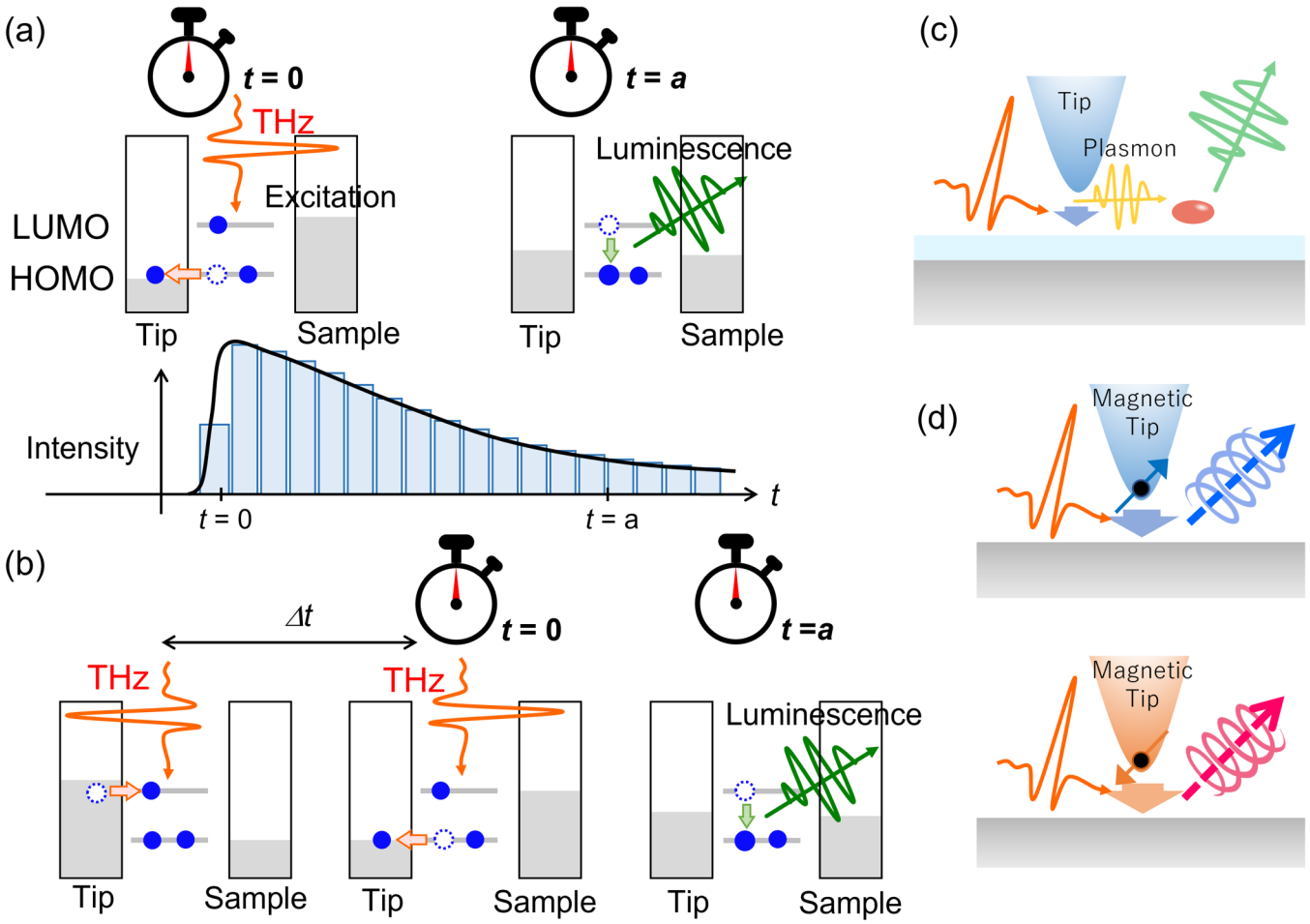

FIG. 5. Possible experiments conducted by THz-STL. (a) Electron tunneling induced by the THz pulse forms the excited state at $t = 0$ and emits luminescence at $t = a$, enabling us to investigate luminescence dynamics. (LUMO: lowest unoccupied molecular orbital, HOMO: highest occupied molecular orbital). The gray color represents the position of the chemical potential of electrons. (b) Formation of the excited states through the sequential tunneling of electrons induced by the THz double pulse with a pulse interval of Δt. (c) THz-induced plasmon emission exciting the luminescence of neighboring molecules. (d) Spin-selective excitation of luminescence in a semiconductor through electron tunneling using a magnetic tip. Luminescence with a circular polarization may be emitted.

to or extracted from the sample with a high temporal resolution. Such manipulation of electron tunneling at the STM nanogap will pave the way for investigating luminescence from molecules and their dynamics. This can also be extended to the observation of chemical reaction dynamics, such as oxidation and reduction. Furthermore, as shown in Fig. 1, many measurement techniques can be combined with THz-STM or THz-STL. These interesting possibilities may be demonstrated in the next few decades to reveal the nanoscale dynamics of the excited states in single molecules, dimers, and solid-state surfaces.

SUMMARY

The fundamentals of THz-STM, recent developments in THz-STL spectroscopy, and its potential for revealing ultrafast excited-state dynamics at the nanoscale are evaluated. THz pulses applied to the STM tip modulate the tip–sample voltage, and net tunneling current can be observed when nonlinearity or asymmetry of the current–voltage characteristic exists in the sample. Similar to DC-STM, THz-STM can induce luminescence, which offers new possibilities for investigating the excited states dynamics and energy dissipation at the nanoscale. THz-STM is a growing field of research as many sophisticated STM techniques are awaiting to be combined with THz pulses, which can provide new research areas and directions in ultrafast nanoscience in the future.

ACKNOWLEDGMENTS

This work is partly supported by the Grants-in-Aid for Scientific Research (Nos. 20H05662, 21H05412, 22H04967, and

20H02653). J.T. is also grateful for the support of the Mitsubishi Foundation (No. 202110024). The authors would like to thank Enago (www.enago.jp) for the English language review.

AUTHOR DECLARATIONS

Conflict of Interest

The authors have no conflicts to disclose.

Author Contributions

Ikufumi Katayama: Conceptualization (equal); Data curation (equal); Formal analysis (equal); Funding acquisition (equal); Investigation (equal); Methodology (equal); Writing – original draft (equal); Writing – review & editing (equal). **Kensuke Kimura:** Conceptualization (equal); Data curation (equal); Formal analysis (equal); Funding acquisition (equal); Investigation (equal); Methodology (equal); Resources (equal); Software (equal); Writing – review & editing (equal). **Hiroshi Imada:** Conceptualization (equal); Funding acquisition (equal); Investigation (equal); Project administration (equal); Supervision (equal); Writing – review & editing (equal). **Yousoo Kim:** Conceptualization (equal); Funding acquisition (equal); Investigation (equal); Project administration (equal); Resources (equal); Supervision (equal); Writing – review & editing (equal). **Jun Takeda:** Conceptualization (equal); Funding acquisition (equal); Investigation (equal); Project administration (equal); Resources (equal); Supervision (equal); Writing – review & editing (equal).

DATA AVAILABILITY

The data that support the findings of this study are available from the corresponding authors upon reasonable request.

REFERENCES

[1]M. Haider, S. Uhlemann, E. Schwan, H. Rose, B. Kabius, and K. Urban, Nature **392**(6678), 768 (1998).
[2]A. Sakdinawat and D. Attwood, Nat. Photonics **4**(12), 840 (2010).
[3]B. Shen, H. Wang, H. Xiong, X. Chen, E. G. T. Bosch, I. Lazić, W. Qian, and F. Wei, Nature **607**(7920), 703 (2022).
[4]T. Hanaguri, C. Lupien, Y. Kohsaka, D. H. Lee, M. Azuma, M. Takano, H. Takagi, and J. C. Davis, Nature **430**(7003), 1001 (2004).
[5]S.-W. Hla and K.-H. Rieder, Annu. Rev. Phys. Chem. **54**(1), 307 (2003).
[6]A. J. Huber, F. Keilmann, J. Wittborn, J. Aizpurua, and R. Hillenbrand, Nano Lett. **8**(11), 3766 (2008).
[7]G. Binnig and H. Rohrer, Surf. Sci. **126**(1), 236 (1983).
[8]Y. Martin and H. K. Wickramasinghe, Appl. Phys. Lett. **50**(20), 1455 (1987).
[9]D. M. Eigler and E. K. Schweizer, Nature **344**(6266), 524 (1990).
[10]R. Wiesendanger, H. J. Güntherodt, G. Güntherodt, R. J. Gambino, and R. Ruf, Phys. Rev. Lett. **65**(2), 247 (1990).
[11]M. Nonnenmacher, M. P. O'Boyle, and H. K. Wickramasinghe, Appl. Phys. Lett. **58**(25), 2921 (1991).
[12]L. Novotny, D. W. Pohl, and B. Hecht, Opt. Lett. **20**(9), 970 (1995).
[13]T. Yokoyama, S. Yokoyama, T. Kamikado, Y. Okuno, and S. Mashiko, Nature **413**(6856), 619 (2001).
[14]T. Kiwa, M. Tonouchi, M. Yamashita, and K. Kawase, Opt. Lett. **28**(21), 2058 (2003).
[15]L. Gross, N. Moll, F. Mohn, A. Curioni, G. Meyer, F. Hanke, and M. Persson, Phys. Rev. Lett. **107**(8), 086101 (2011).
[16]F. Mohn, L. Gross, N. Moll, and G. Meyer, Nat. Nanotechnol. **7**(4), 227 (2012).
[17]R. Zhang, Y. Zhang, Z. C. Dong, S. Jiang, C. Zhang, L. G. Chen, L. Zhang, Y. Liao, J. Aizpurua, Y. Luo, J. L. Yang, and J. G. Hou, Nature **498**(7452), 82 (2013).
[18]J. Zhang, P. Chen, B. Yuan, W. Ji, Z. Cheng, and X. Qiu, Science **342**(6158), 611, (2013).
[19]A. Laraoui, H. Aycock-Rizzo, Y. Gao, X. Lu, E. Riedo, and C. A. Meriles, Nat. Commun. **6**(1), 8954 (2015).
[20]J. Guo, K. Bian, Z. Lin, and Y. Jiang, J. Chem. Phys. **145**(16), 160901 (2016).
[21]D. N. Basov, M. M. Fogler, and F. J. García de Abajo, Science **354**(6309), aag1992, (2016).
[22]Y. F. Dufrêne, T. Ando, R. Garcia, D. Alsteens, D. Martinez-Martin, A. Engel, C. Gerber, and D. J. Müller, Nat. Nanotechnol. **12**(4), 295 (2017).
[23]S. Meyer, M. Perini, S. von Malottki, A. Kubetzka, R. Wiesendanger, K. von Bergmann, and S. Heinze, Nat. Commun. **10**(1), 3823 (2019).
[24]S. Liu, B. Cirera, Y. Sun, I. Hamada, M. Muller, A. Hammud, M. Wolf, and T. Kumagai, Nano Lett. **20**(8), 5879 (2020).
[25]R. Péchou, S. Jia, J. Rigor, O. Guillermet, G. Seine, J. Lou, N. Large, A. Mlayah, and R. Coratger, ACS Photonics **7**(11), 3061 (2020).
[26]K. J. P. Jacobs, H. Murakami, F. Murakami, K. Serita, E. Beyne, and M. Tonouchi, Nat. Electron. **4**(3), 202 (2021).
[27]F.-F. Kong, X.-J. Tian, Y. Zhang, Y. Zhang, G. Chen, Y.-J. Yu, S.-H. Jing, H.-Y. Gao, Y. Luo, J.-L. Yang, Z.-C. Dong, and J. G. Hou, Nat. Nanotechnol. **17**(7), 729 (2022).
[28]J. G. Simmons, J. Appl. Phys. **34**(6), 1793 (1963).
[29]F. Moresco and A. Gourdon, Proc. Natl. Acad. Sci. U.S.A. **102**(25), 8809 (2005).
[30]A. van Houselt and H. J. W. Zandvliet, Rev. Mod. Phys. **82**(2), 1593 (2010).
[31]M. Rashidi, J. A. J. Burgess, M. Taucer, R. Achal, J. L. Pitters, S. Loth, and R. A. Wolkow, Nat. Commun. **7**(1), 13258 (2016).
[32]Y. Terada, S. Yoshida, O. Takeuchi, and H. Shigekawa, Nat. Photonics **4**(12), 869 (2010).
[33]S. Yoshida, Y. Aizawa, Z. H. Wang, R. Oshima, Y. Mera, E. Matsuyama, H. Oigawa, O. Takeuchi, and H. Shigekawa, Nat. Nanotechnol. **9**(8), 588 (2014).
[34]S. Grafström, J. Appl. Phys. **91**(4), 1717 (2002).
[35]M. Tonouchi, Nat. Photonics **1**(2), 97 (2007).
[36]T. Kampfrath, K. Tanaka, and K. A. Nelson, Nat. Photonics **7**(9), 680 (2013).
[37]D. M. Mittleman, J. Appl. Phys. **122**(23), 230901 (2017).
[38]T. L. Cocker, V. Jelic, M. Gupta, S. J. Molesky, J. A. J. Burgess, G. D. L. Reyes, L. V. Titova, Y. Y. Tsui, M. R. Freeman, and F. A. Hegmann, Nat. Photonics **7**(8), 620 (2013).
[39]K. Yoshioka, I. Katayama, Y. Minami, M. Kitajima, S. Yoshida, H. Shigekawa, and J. Takeda, Nat. Photonics **10**(12), 762 (2016).
[40]T. L. Cocker, D. Peller, P. Yu, J. Repp, and R. Huber, Nature **539**(7628), 263 (2016).
[41]T. L. Cocker, V. Jelic, R. Hillenbrand, and F. A. Hegmann, Nat. Photonics **15**(8), 558 (2021).
[42]T. Tachizaki, K. Hayashi, Y. Kanemitsu, and H. Hirori, APL Mater. **9**(6), 060903 (2021).
[43]V. Jelic, K. Iwaszczuk, P. H. Nguyen, C. Rathje, G. J. Hornig, H. M. Sharum, J. R. Hoffman, M. R. Freeman, and F. A. Hegmann, Nat. Phys. **13**(6), 591 (2017).
[44]M. Abdo, S. Sheng, S. Rolf-Pissarczyk, L. Arnhold, J. A. J. Burgess, M. Isobe, L. Malavolti, and S. Loth, ACS Photonics **8**(3), 702 (2021).
[45]L. Wang, Y. Xia, and W. Ho, Science **376**(6591), 401, (2022).
[46]S. Yoshida, H. Hirori, T. Tachizaki, K. Yoshioka, Y. Arashida, Z.-H. Wang, Y. Sanari, O. Takeuchi, Y. Kanemitsu, and H. Shigekawa, ACS Photonics **6**(6), 1356 (2019).
[47]S. Yoshida, Y. Arashida, H. Hirori, T. Tachizaki, A. Taninaka, H. Ueno, O. Takeuchi, and H. Shigekawa, ACS Photonics **8**(1), 315 (2021).
[48]D. Peller, L. Z. Kastner, T. Buchner, C. Roelcke, F. Albrecht, N. Moll, R. Huber, and J. Repp, Nature **585**(7823), 58 (2020).

[49]D. Peller, C. Roelcke, L. Z. Kastner, T. Buchner, A. Neef, J. Hayes, F. Bonafé, D. Sidler, M. Ruggenthaler, A. Rubio, R. Huber, and J. Repp, Nat. Photonics **15**(2), 143 (2021).
[50]J. Takeda and I. Katayama, Nat. Photonics **15**(2), 70 (2021).
[51]K. Yoshioka, I. Igarashi, S. Yoshida, Y. Arashida, I. Katayama, J. Takeda, and H. Shigekawa, Opt. Lett. **44**(21), 5350 (2019).
[52]M. Muller, N. Martin Sabanes, T. Kampfrath, and M. Wolf, ACS Photonics **7**(8), 2046 (2020).
[53]M. Garg and K. Kern, Science **367**(6476), 411, (2020).
[54]M. Garg, A. Martin-Jimenez, M. Pisarra, Y. Luo, F. Martín, and K. Kern, Nat. Photonics **16**(3), 196 (2022).
[55]M. Garg, A. Martin-Jimenez, Y. Luo, and K. Kern, ACS Nano **15**(11), 18071 (2021).
[56]Y. Arashida, H. Mogi, M. Ishikawa, I. Igarashi, A. Hatanaka, N. Umeda, J. Peng, S. Yoshida, O. Takeuchi, and H. Shigekawa, ACS Photonics **9**, 3156 (2022).
[57]K. Kimura, Y. Morinaga, H. Imada, I. Katayama, K. Asakawa, K. Yoshioka, Y. Kim, and J. Takeda, ACS Photonics **8**(4), 982 (2021).
[58]H. Imada, K. Miwa, M. Imai-Imada, S. Kawahara, K. Kimura, and Y. Kim, Nature **538**(7625), 364 (2016).
[59]K. Kimura, K. Miwa, H. Imada, M. Imai-Imada, S. Kawahara, J. Takeya, M. Kawai, M. Galperin, and Y. Kim, Nature **570**(7760), 210 (2019).
[60]Y. Luo, V. Jelic, G. Chen, P. H. Nguyen, Y.-J. R. Liu, J. A. M. Calzada, D. J. Mildenberger, and F. A. Hegmann, Phys. Rev. B **102**(20), 205417 (2020).
[61]U. S. Sainadh, H. Xu, X. Wang, A. Atia-Tul-Noor, W. C. Wallace, N. Douguet, A. Bray, I. Ivanov, K. Bartschat, A. Kheifets, R. T. Sang, and I. V. Litvinyuk, Nature **568**(7750), 75 (2019).
[62]K. Yoshioka, I. Katayama, Y. Arashida, A. Ban, Y. Kawada, K. Konishi, H. Takahashi, and J. Takeda, Nano Lett. **18**(8), 5198 (2018).
[63]F. Mooshammer, M. A. Huber, F. Sandner, M. Plankl, M. Zizlsperger, and R. Huber, ACS Photonics **7**(2), 344 (2020).
[64]J. Hebling, G. Almási, I. Z. Kozma, and J. Kuhl, Opt. Express **10**(21), 1161 (2002).
[65]K.-L. Yeh, M. C. Hoffmann, J. Hebling, and K. A. Nelson, Appl. Phys. Lett. **90**, 171121 (2007).
[66]H. Hirori, A. Doi, F. Blanchard, and K. Tanaka, Appl. Phys. Lett. **98**, 091106 (2011).
[67]P. Wan, L.-M. Yang, and J. Liu, Opt. Express **21**(24), 29854 (2013).
[68]I. J. Graumann, A. Diebold, C. G. E. Alfieri, F. Emaury, B. Deppe, M. Golling, D. Bauer, D. Sutter, C. Kränkel, C. J. Saraceno, C. R. Phillips, and U. Keller, Opt. Express **25**(19), 22519 (2017).
[69]M. Nagai, M. Jewariya, Y. Ichikawa, H. Ohtake, T. Sugiura, Y. Uehara, and K. Tanaka, Opt. Express **17**(14), 11543 (2009).
[70]S. E. Ammerman, V. Jelic, Y. Wei, V. N. Breslin, M. Hassan, N. Everett, S. Lee, Q. Sun, C. A. Pignedoli, P. Ruffieux, R. Fasel, and T. L. Cocker, Nat. Commun. **12**(1), 6794 (2021).
[71]S. Li, S. Chen, J. Li, R. Wu, and W. Ho, Phys. Rev. Lett. **119**(17), 176002 (2017).
[72]S. Liu, A. Hammud, I. Hamada, M. Wolf, M. Müller, and T. Kumagai, Sci. Adv. **8**, eabq5682 (2022).
[73]M. Plankl, P. E. Faria Junior, F. Mooshammer, T. Siday, M. Zizlsperger, F. Sandner, F. Schiegl, S. Maier, M. A. Huber, M. Gmitra, J. Fabian, J. L. Boland, T. L. Cocker, and R. Huber, Nat. Photonics **15**(8), 594 (2021).
[74]P. Merino, C. Große, A. Rosławska, K. Kuhnke, and K. Kern, Nat. Commun. **6**, 8461 (2015).
[75]L. Zhang, Y.-J. Yu, L.-G. Chen, Y. Luo, B. Yang, F.-F. Kong, G. Chen, Y. Zhang, Q. Zhang, Y. Luo, J.-L. Yang, Z.-C. Dong, and J. G. Hou, Nat. Commun. **8**, 580 (2017).
[76]A. Rosławska, P. Merino, C. Große, C. C. Leon, O. Gunnarsson, M. Etzkorn, K. Kuhnke, and K. Kern, Nano Lett. **18**(6), 4001 (2018).
[77]H. Hirori, K. Shinokita, M. Shirai, S. Tani, Y. Kadoya, and K. Tanaka, Nat. Commun. **2**, 594 (2011).
[78]B. C. Pein, W. Chang, H. Y. Hwang, J. Scherer, I. Coropceanu, X. Zhao, X. Zhang, V. Bulović, M. Bawendi, and K. A. Nelson, Nano Lett. **17**(9), 5375 (2017).
[79]R. Berndt, J. K. Gimzewski, and P. Johansson, Phys. Rev. Lett. **67**(27), 3796 (1991).
[80]K. Kuhnke, C. Große, P. Merino, and K. Kern, Chem. Rev. **117**(7), 5174 (2017).
[81]B. Doppagne, M. C. Chong, H. Bulou, A. Boeglin, F. Scheurer, and G. Schull, Science **361**(6399), 251, (2018).
[82]Z. He, Z. Han, J. Yuan, A. M. Sinyukov, H. Eleuch, C. Niu, Z. Zhang, J. Lou, J. Hu, D. V. Voronine, and M. O. Scull, Sci. Adv. **5**(10), aau8763 (2019).
[83]J. J. Baumberg, Nano Lett. **22**(14), 5859 (2022).
[84]H. Imada, K. Miwa, M. Imai-Imada, S. Kawahara, K. Kimura, and Y. Kim, Phys. Rev. Lett. **119**(1), 013901 (2017).
[85]S. Cao, A. Rosławska, B. Doppagne, M. Romeo, M. Féron, F. Chérioux, H. Bulou, F. Scheurer, and G. Schull, Nat. Chem. **13**(8), 766 (2021).
[86]G. Reecht, F. Scheurer, V. Speisser, Y. J. Dappe, F. Mathevet, and G. Schull, Phys. Rev. Lett. **112**(4), 047403 (2014).
[87]S. Yamamoto, H. Imada, and Y. Kim, Phys. Rev. Lett. **128**, 206804 (2022).